

RESEARCH PAPER



# Identification of 1*H*-pyrazolo[3,4-*b*]pyridine derivatives as novel and potent TBK1 inhibitors: design, synthesis, biological evaluation, and molecular docking study

Yin Sun<sup>a,b,\*</sup>, Haotian Tang<sup>b,c,\*</sup>, Xiaoyan Wang<sup>a,b,\*</sup>, Fang Feng<sup>b</sup>, Tiantian Fan<sup>b,c</sup>, Dongmei Zhao<sup>a</sup>, Bing Xiong<sup>b</sup>,  
Hua Xie<sup>b,c,d</sup> and Tongchao Liu<sup>b</sup>

<sup>a</sup>Key Laboratory of Structure-Based Drug Design and Discovery of Ministry of Education, Shenyang Pharmaceutical University, Shenyang, P. R. China; <sup>b</sup>Shanghai Institute of Materia Medica, Chinese Academy of Sciences, Shanghai, P. R. China; <sup>c</sup>University of Chinese Academy of Sciences, Beijing, P. R. China; <sup>d</sup>Zhongshan Institute for Drug Discovery, Shanghai Institute of Materia Medica, Chinese Academy of Sciences, Shanghai, P. R. China

## SUBSTRACT

TANK-binding kinase 1 (TBK1), a noncanonical member of the inhibitor-kappaB kinases (IKKs) family, plays a vital role in coordinating the signalling pathways of innate immunity, involving in the process of neuro-inflammation, auto-phagy, and oncogenesis. In current study, based on rational drug design strategy, we discovered a series of 1*H*-pyrazolo[3,4-*b*]pyridine derivatives as potent TBK1 inhibitors and dissected the structure–activity relationships (SARs). Through the several rounds of optimisation, compound **15y** stood out as a potent inhibitor on TBK1 with an IC<sub>50</sub> value of 0.2 nM and also displayed good selectivity. The mRNA detection of TBK1 downstream genes showed that compound **15y** effectively inhibited TBK1 downstream IFN signalling in stimulated THP-1 and RAW264.7 cells. Meanwhile, compound **15y** exhibited a micromolar antiproliferation effect on A172, U87MG, A375, A2058, and Panc0504 cell lines. Together, current results provided a promising TBK1 inhibitor **15y** as lead compound for immune- and cancer-related drug discovery.

## ARTICLE HISTORY

Received 1 March 2022  
Revised 18 April 2022  
Accepted 21 April 2022

## KEYWORDS

TBK1 inhibitors; 1*H*-pyrazolo[3,4-*b*]pyridine; structure–activity relationships (SARs); immune response; cancer therapy

## 1. Introduction

The inhibitor-kappaB kinases (IKKs), a conserved serine/threonine kinases family, is involved in the metabolism, immune response, and tumorigenesis.<sup>1–3</sup> The five members of the IKKs comprise three canonical kinases: IKK $\alpha$ , IKK $\beta$ , and IKK $\gamma$  (NEMO), and two noncanonical ones: TANK-binding kinase 1 (TBK1) and IKK $\epsilon$ .<sup>4</sup> Except IKK $\gamma$  possessing a nonenzymatic regulatory component, the other canonical and noncanonical IKK kinases share similar structure characteristics: an N-terminal (Ser/Thr) catalytic kinase domain (KD) containing the ATP-binding site followed closely a ubiquitin-like domain (ULD), a C-terminal domain (CTD) facilitating the formation of multi-enzyme complexes by mediating the binding of adaptor proteins and a helical scaffold dimerisation domain (SDD) maintaining structural integrity.<sup>5</sup> Moreover, the KD of TBK1 presents 49% identity and 65% similarity to that of IKK $\epsilon$ . Thus, in order to further exploring the biological function of TBK1, development of a highly selective TBK1 inhibitor has become an urgent need. The past years has witnessed an exponential increase in the number of researchers who try to develop a selective TBK1 inhibitor due to the importance of TBK1 in cell signalling pathways.

TBK1, also known as NF- $\kappa$ B-activating kinase (NAK) or T2K, which is widely expressed in all tissues, has emerged as a prospective therapeutic target, playing increasingly momentous roles

in metabolic diseases, autoimmune diseases, and cancer.<sup>3,6,7</sup> Several studies have found that TBK1 is positively regulated by RIG-I like receptors (RLRs), Toll-like receptors (TLRs) and the stimulator of interferon genes (STING) protein.<sup>8–10</sup> The activation of TBK1 is essential for the production of type I interferon (IFN) *in vivo*. The activated TBK1 can regulate IFN signal by phosphorylating interferon regulatory factor 3/7 (IRF3/7) and then dimerising them into the nucleus, thus inducing the expression of pro-inflammatory and anti-viral genes. In addition to mediating the innate immune response, TBK1 also plays a critical role in cancer therapy. A growing number of studies have suggested that aberrant activation of TBK1 is closely associated to the occurrence and development of cancer, such as lung,<sup>11</sup> breast,<sup>12</sup> colon,<sup>13</sup> bladder,<sup>14</sup> glioblastoma,<sup>6,15</sup> melanoma,<sup>16</sup> and pancreas<sup>17,18</sup> cancers. Knockdown experiments have identified that TBK1 is a synthetic lethal partner of oncogenic mutated oncogenic Kirsten rat sarcoma 2 viral oncogene homolog (KRAS).<sup>19</sup> Although TBK1 has been proposed as a target of inflammatory, autoimmune and metabolic disorders as well as cancer, the related mechanisms remain unclear to large extent. Therefore, tool molecules need to be developed urgently for further revealing TBK1 biological functions involving the correlative network of cell signals of immune response and cancer.

**CONTACT** Dongmei Zhao  [medchemzhao@163.com](mailto:medchemzhao@163.com)  Shenyang Pharmaceutical University, 103 Wenhua Lu, Shenyang 110016, P. R. China; Bing Xiong  [bxiong@simm.ac.cn](mailto:bxiong@simm.ac.cn); Hua Xie  [hxie@simm.ac.cn](mailto:hxie@simm.ac.cn); Tongchao Liu  [tongchao\\_liu@simm.ac.cn](mailto:tongchao_liu@simm.ac.cn)  Shanghai Institute of Materia Medica, Chinese Academy of Sciences, 555 Zuchongzhi Road, Shanghai 201203, P. R. China

\*Yin Sun, Haotian Tang, and Xiaoyan Wang contributed equally to this work.

 Supplemental data for this article can be accessed [here](#).

© 2022 The Author(s). Published by Informa UK Limited, trading as Taylor & Francis Group.

This is an Open Access article distributed under the terms of the Creative Commons Attribution License (<http://creativecommons.org/licenses/by/4.0/>), which permits unrestricted use, distribution, and reproduction in any medium, provided the original work is properly cited.

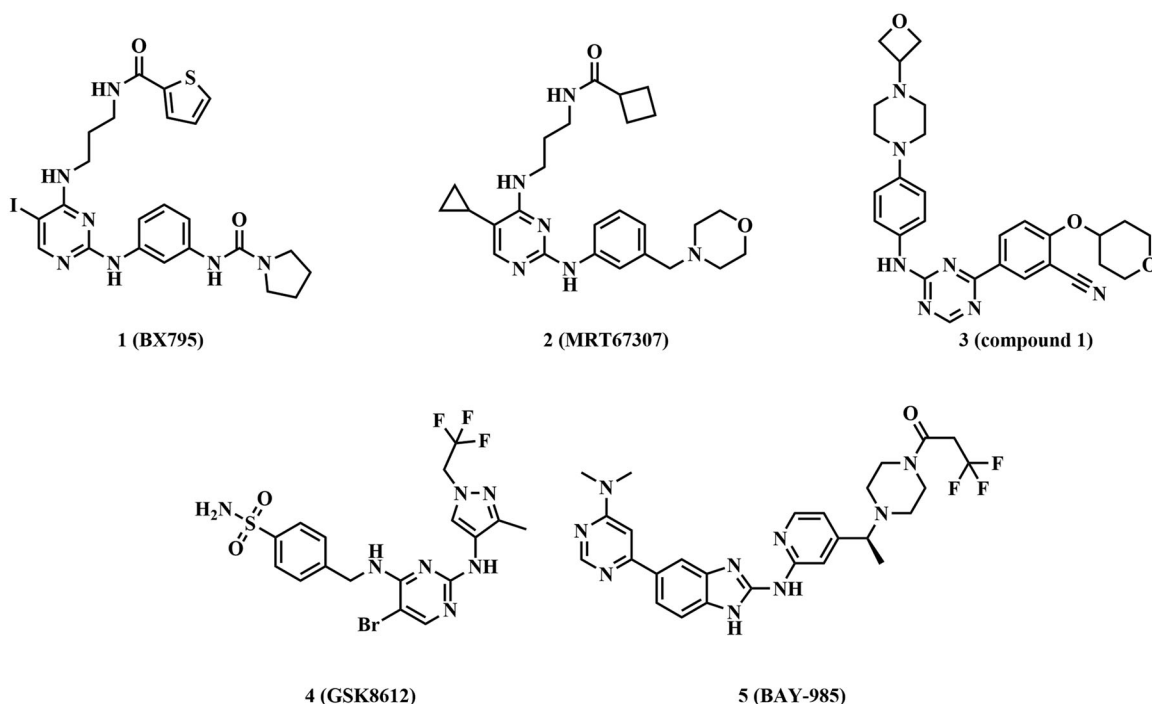


**Figure 1.** Structures of potent TBK1 inhibitors.

Currently, there are no TBK1 inhibitors in the clinical trials. A few representative small molecule inhibitors of TBK1 were depicted in **Figure 1**. **BX795** (**1**) was initially designed as an inhibitor of PDK1, and then researchers found that it displayed nanomolar activity on TBK1 ( $IC_{50} = 2$  nM) and IKK $\epsilon$  ( $IC_{50} = 9$  nM).<sup>20–22</sup> Although **BX795** is a multi-target kinase inhibitor, the researchers obtained the co-crystal structure of **BX795** and TBK1 (PDB ID 4IM2), which revealed the binding mode of inhibitors of this type and TBK1, laying the foundation for the follow-up studies. **BX795** was optimised by Clark group in the University of Dundee to generate **MRT67307** (**2**),<sup>23,24</sup> which also presented robust suppressive activity on TBK1 ( $IC_{50} = 19$  nM) and IKK $\epsilon$  ( $IC_{50} = 160$  nM). Furthermore, it possessed almost no inhibitory effect on IKK $\alpha$  and IKK $\beta$  at a concentration of 10  $\mu$ M. **Compound 1** (**3**),<sup>25</sup> a potent TBK1/IKK $\epsilon$  inhibitor, showed the  $IC_{50}$  values of 1.0 nM and 5.6 nM against TBK1 and IKK $\epsilon$ , respectively. It could enhance the response to PD-1 blockade and effectively predict the tumour response *in vivo*. In recent years, two TBK1 inhibitors **GSK8612** (**5**)<sup>26</sup> and **BAY-985** (**6**),<sup>27</sup> reported by GlaxoSmithKline and Bayer, respectively, served as ideal probes to further dissect the biological function of TBK1 in models of immunity and cancer. **GSK8612** exhibited an excellent kinase selectivity with  $pK_d$  of 8.0. **BAY-985** showed strong inhibition activity on TBK1 ( $IC_{50} = 2$  nM) and IKK $\epsilon$  ( $IC_{50} = 2$  nM); however, it displayed weak anti-tumour activity in a xenograft model of SK-MEL-2 human melanoma cell line.

### 1.1. Rationale of the design

Based on the in-house kinase compound library, we performed a TBK1 screening campaign and screened out the azaindole skeleton compound **URMC-099** with the inhibition rate of 75.3% on TBK1 at the concentration of 10  $\mu$ M. In an effort to gain potent TBK1 inhibitors, we first docked and analysed the binding mode of **URMC-099** and TBK1 (PDB code 4IWQ) (**Figure 2**). The interactions showed that the NH of indole formed a hydrogen bond with Asp157 of DFG motif, the NH and N of azaindole

formed two hydrogen bonds with hinge residue Glu87 and Cys89, and polar-fragment methylpiperazine extended to the solvent region. On the basis of the synthesis accessibility and the binding mode of azaindole, nitrogen atom was introduced at the 2-position of pyrrole ring according to the principle of bioisostere, which was expected to enhance the anchoring effect between NH and Glu87 of hinge region under the strong electron-withdrawing function of pyrazole N atom. Therefore, we designed and synthesised the compound **6** (**15a**, 83.0% inhibition @ 10  $\mu$ M) as a hit. The docking study displayed that the binding model of **6** was same as that of **URMC-099**. Subsequently, two modification sites ( $R^1$  and  $R^2$ ) were chosen to guide the design and synthesis of these 1*H*-pyrazolo[3,4-*b*]pyridine derivatives (**Figure 3**).

On the basis of above analysis and with the aid of computer-aided drug design (CADD), we described here our efforts to discover a novel class of potent TBK1 inhibitors by applying structure-based drug design (SBDD). In the light of the designed pyrazolopyridine core, we fixed the methylpiperazine fragment in the solvent region and first investigated the structure of the indole ring extending to the DFG region. Hereby, two-series compounds were designed: one (compounds **12a–12i**) was that we employed fragment splicing strategy to introduce the similar alkylamino side chain of **BX795** and explore the chain length; the other (compounds **15a–15f**) was that allowing for the hydrogen bond between NH of indole ring and Asp157, we modified the indole ring and analysed the importance of the hydrogen bond. Unfortunately, the first-series compounds had little activity on TBK1. We speculated that the main reason might be that the binding mode of anchoring region was changed from pyridopyrazole to aminopyrazole as a result of the introduction of alkylamine fragment. Fortunately, the second-series compound **15e** exhibited strong inhibitory activity on TBK1 with an  $IC_{50}$  value of 75.3 nM after replacing indole ring with 1-isopropylbenzimidazole, which suggested compound **15e** became an appropriate lead in hit to lead stage. Meanwhile, we concluded that Asp157 was an important amino acid for TBK1-dependent activity. Subsequently, we

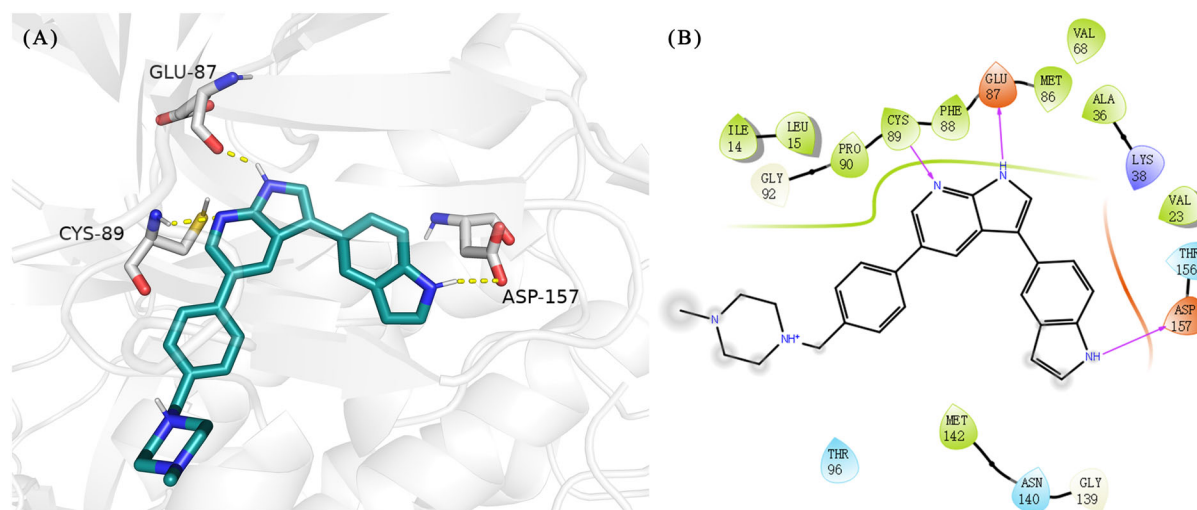


**Figure 2.** (A) The binding mode of URMC-099 (coloured by element with carbons in teal) in the TBK1 active site. The kinase was depicted in white cartoon, and interactions were illustrated with yellow dashed lines. (B) 2D diagram of the interaction between URMC-099 and TBK1.

carried out the next structural modification around sites R<sup>1</sup> and R<sup>2</sup>. With the **15i** (IC<sub>50</sub> = 8.5 nM) and **15t** (IC<sub>50</sub> = 0.8 nM) were obtained, further optimisation and structure–activity relationships (SARs) study were conducted, which led to identification of a potent TBK1 inhibitor **15y** (IC<sub>50</sub> = 0.2 nM). The design, synthesis, biological evaluation, and docking study of these inhibitors are discussed in this manuscript.

## 2. Materials and methods

### 2.1. Chemistry

All reagents used were commercially available without further purification. Solvents were purified according to standard procedures. Flash chromatography was performed on silica gel (300–400 mesh ASTM) and monitored by thin layer chromatography (TLC) on HSGF-254 (10–40 μm) TLC plates. Nuclear magnetic resonance (NMR) data were collected on a Varian Mercury-300 High Performance Digital FT-NMR, a Varian Mercury-400 High Performance Digital FT-NMR, a Bruker Ultrashield 500 NMR, or an Agilent 1260 Prospekt 2 Bruker Ascend 600 NMR. HRMS were carried out on a Thermo Finnigan MAT-95 spectrometer (for EI), or on a Waters, Q-ToF Ultima Global spectrometer (for ESI). The purity of compounds was determined by Gilson-215 high performance liquid chromatography (HPLC) using an YMC ODS3 column (50 mm × 4.6 mm, 5 μm) and confirmed to be more than 95%, monitored by UV absorption at 214 and 254 nm. Conditions were as follows: CH<sub>3</sub>CN/H<sub>2</sub>O eluent at 2.5 ml/min flow containing 0.1% trifluoroacetic acid (TFA) at 35 °C, 8 min, gradient 5% CH<sub>3</sub>CN to 95% CH<sub>3</sub>CN.

### 2.2. Biological evaluation

#### 2.2.1. Enzymatic assay

The TBK1 kinase activity of the novel compounds were evaluated by the FRET-based Z'-LYTE assay (Invitrogen, PV3178) following the manufacture's instruction. Briefly, test compounds were added to the mixture of 4 ng of TBK1 kinase (Thermo Scientific, A31513) into each well of a 384 well-plate (Corning, 3514) and to react with 4 μM substrate peptide in 100 μM ATP for 1 h at room temperature. Subsequently 5 μL of development reagent was added

into each well for further 1 h until 5 μL of stop reagents were added to eliminate the reaction. Fluorescence signals were measured by SpectraMax Paradigm (Molecular Devices).

#### 2.2.2. Kinase selectivity profile

Compound **15y** was evaluated for their inhibitory activities against 31 kinases at a single concentration (1 μM). Two different assay platforms were available for profiling—activity and binding. The Z'-LYTE and Adapta kinase activity assays were used most extensively for profiling and a smaller subset of kinases might be profiled using the LanthaScreen Eu Kinase Binding Assays.

#### 2.2.3. mRNA detection of TBK1 downstream genes

Human monocyte THP-1 cells and murine macrophage RAW264.7 cells were purchased from ATCC and were cultured in RPMI or DMEM medium supplement with 10% FBS. Both cells were seeded overnight and were pre-treated with different compounds for 2 h, and then were stimulated with either 0.1 μg/mL poly(I:C) or 1 μg/mL LPS for 3 h, respectively. Total RNA was extracted from cultured cells using EZ-press RNA purification kit (EZBioscience, B0004DP). Afterwards, extracted RNA was reverse transcribed into first strand cDNA by HiScript III RT Super Mix for qPCR (Vazyme, R323-00) and was applied for quantitative real-time polymerase chain reaction (RT-PCR) via ChamQ Universal SYBR qPCR Master Mix (Vazyme, Q711-02) with the BIO-RAD CFX96 C1000 touch thermal cycler. The amplification conditions were followed by protocol of SYBR qPCR Master Mix (Vazyme, Q711-02). All RT-PCR experiments were tested in triplicate, and the relative expression of genes were normalised to the control gene β-actin using the 2-ΔΔCq method. Data are shown in mean ± SD value, and t-test was performed to compare the significance between control group and treated groups by GraphPad 8.0.

The primers used for RT-PCR were as follows: *ifnb* (human)-Forward: GGCACAACAGGTAGTAGGCG; *ifnb* (human)-Reverse: GTGGAGAAGCACACAGGAGA; *cxcl-10* (human)-Forward: CCTGCAAGCCAAATTTGTCCA; *cxcl-10* (human)-Reverse: TGTGGTCCATCCTTGAAGC; *β-actin* (human)-Forward: GAGCACAGAGCCTCGCCTTT; *β-actin* (human)-Reverse: TCATCATCCATGGTGAGCTGGC; *ifnb* (mouse)-Forward: CAACAGCTACGCCTGGATGG; *ifnb* (mouse)-Reverse: CCTGCAACCACCACTCATT; *cxcl-10* (mouse)-Forward: AGT

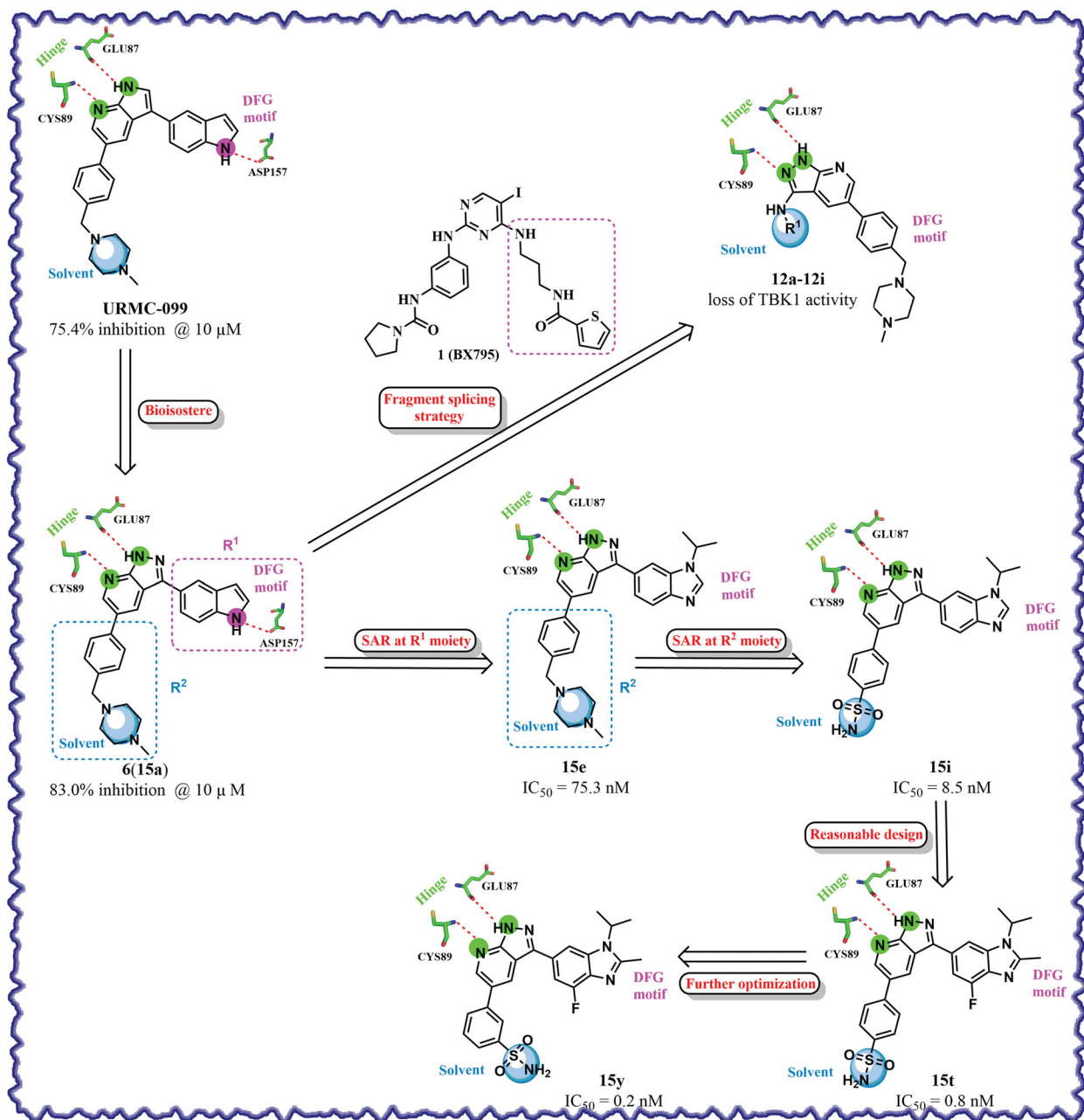


Figure 3. Design and modification strategies of novel TBK1 inhibitors.

GCTGCCGTCATTTTCTG; *cxl-10* (mouse)-Reverse: TCCTATGGCCCT CATTCTCA;  $\beta$ -actin (mouse)-Forward: GTCGAGTCGCGTCCACC;  $\beta$ -actin (mouse)-Reverse: ACGATGGAGGGGAATACAGC.

#### 2.2.4. Antiproliferative activity of compound 15y

A172, U87MG, A375, A2058, and Panc0504 cell lines were obtained from ATCC and cultured in indicated medium according to ATCC's instructions. Cells were seeded in 96 well-plates at a density of around 2000 cells per well one day prior to administration to increasing doses of indicated compounds. After 72 h of treatment, cells were washed with PBS and were fixed by 10% trichloroacetic acid before stained by sulphorhodamine B (SRB) solution. Unstained SRB were washed away by 1% acetic acid to reduce background signals. A Tris-based solution (10 mM) were used to dissolve stained SRB and the absorbance at 540 nm was measured with SpectraMax Paradigm (Molecular Devices).

Inhibition rate was calculated by the relative absorbance value of test compound wells with the average of control wells plus 100%.

#### 2.2.5. Molecular docking

The TBK1 crystal structure (PDB code: 4IWQ), which was downloaded from the protein data bank (<https://www.rcsb.org/>), was processed with the Protein Preparation Wizard in the Schrödinger suite. The protein structure was adjusted and modified, followed by adding hydrogen atoms, deleting solvent water molecules, and defining right bonds orders using Prime. The protonation and tautomeric states of Asp, Lys, and His were assigned at pH 7.4 state. Afterward, all hydrogen atoms of TBK1 complexes were optimized with OPLS\_2005 force field, which minimized and converged heavy atoms to an RMSD of 0.3. The four selected inhibitors were prepared by using LigPrep from the Schrödinger suite with the OPLS\_2005 force field. The structure of inhibitors

was also adjusted and modified, followed by adding all hydrogen atoms, checking the bond order and atom types. The prepared protein ligand complex was imported into Glide 9.7, which defined it as the receptor structure with size box (15 Å × 15 Å × 15 Å). Based on the OPLS\_2005 force field, the grid of TBK1 crystal structure was generated. The standard precision (SP) mode was set for docking studies without constrained binding to gain results.

### 3. Results and discussion

#### 3.1. Chemistry

Target compounds **12a–12i** and **15a–15aa** were synthesised in a few steps from the key intermediate **9**, an pyrazolo[3,4-b]pyridine core protected with SEM. The key intermediate **9** was prepared by a previously reported synthetic route, which was optimised moderately.<sup>28,29</sup> Then, palladium-catalysed C-N coupling reaction was utilised to obtain corresponding intermediates **10a–10i**. Subsequently, a palladium-catalysed Suzuki reaction between **10a–10i** and 1-methyl-4-[4-(4,4,5,5-tetramethyl-1,3,2-dioxaborolan-2-yl)benzyl]piperazine were conducted to get intermediates **11a–11i**, and then the SEM protecting group was removed to yield the desired products **12a–12i** (Scheme 1).

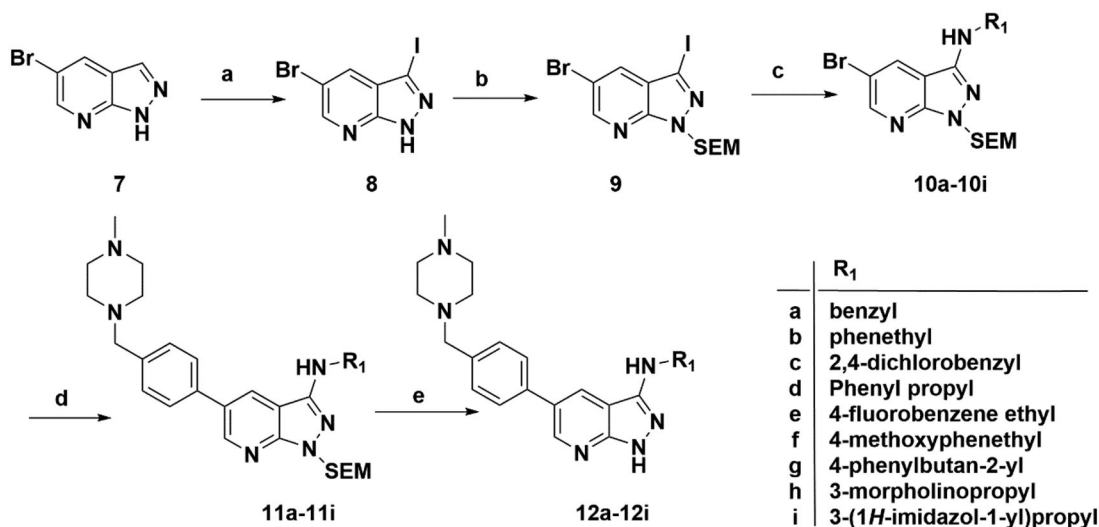
Similarly, after two-step palladium-catalysed Suzuki reactions of intermediate **9** and the removal of the SEM group, the desired products **15a–15f** were obtained (Scheme 2).

For the synthesis of target compounds **15g–15k** (Scheme 3), 5-bromo-N-isopropyl-2-nitroaniline (**16**) was used as the starting

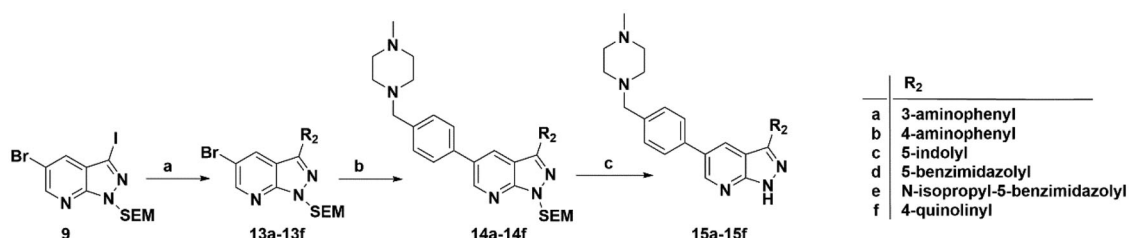
material. Compound **16** was reduced to intermediate **17** by iron powder, followed by the retaining ring reaction with formic acid obtained intermediate **18**, which were converted to intermediate **19** through bis(pinacolato)diboron reaction. Treatment of intermediate **19** with two-step palladium-catalysed Suzuki reactions, followed removing the SEM protecting group to afford end-product **15g–15k**.

Intermediates **26**, **30**, **34**, **38**, and **43** were prepared according to the procedures described in Schemes 4–8. Cyclopropylamine (**22**) was condensed with acetic anhydride to gain intermediate **23**, which was further substituted to get intermediate **24**. Compound **25** was synthesised by the cyclisation of intermediate **24** under basic conditions. Finally, the key intermediate **26** was prepared by Miyaura borylation reaction from the intermediate **25**. The intermediate **30** was afforded from 4-bromo-2,6-difluoroaniline (**27**) via acetylation, cyclisation, and Miyaura borylation reaction. Treatment of 4-bromo-2,6-difluorobenzaldehyde (**31**) with hydrazine hydrate afforded intermediate **32**, then **32** was protected with SEM group to provide intermediate **33**, which further reacted with bis(pinacolato)diboron to yield the key intermediate **34**. The key intermediate **38** was prepared by reduction, cyclisation, and Miyaura borylation reaction with the starting material 4-bromo-2-fluoro-6-nitrophenol (**35**). 4-Bromo-2-fluoro-6-nitroaniline (**39**) yielded the key intermediate **43** via reduction, cyclisation, isopropyl substitution, and Miyaura borylation reaction.

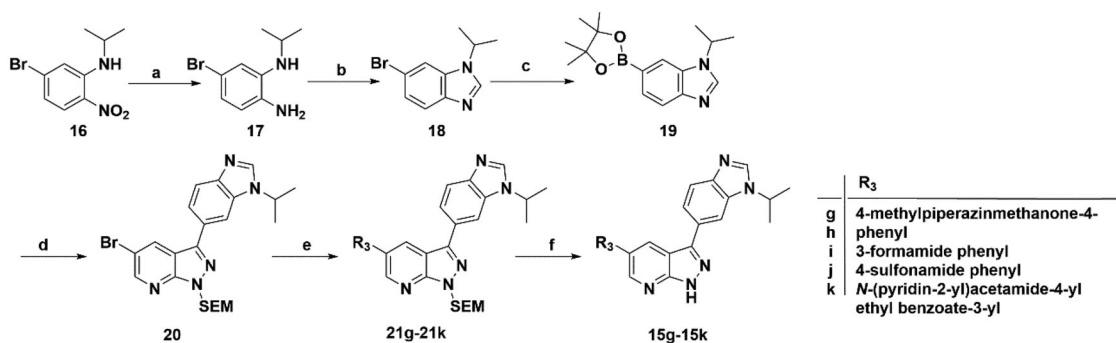
As depicted in Schemes 9 and 10, target compounds **15l–15ab** were prepared by using procedures similar to those described in Schemes 1 and 2, and for compound **15ab**, azaindole core (**46**) was used instead of pyrazolo[3,4-b]pyridine core (**7**).



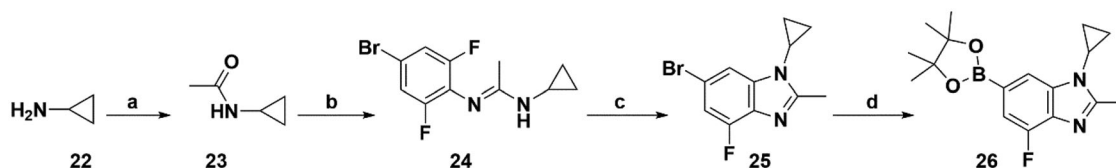
**Scheme 1.** Synthesis of target compounds **12a–12i**. Reagents and conditions: (a) NIS, DMF, 80 °C, 8 h; (b) NaH, SEM-Cl, DMF, 0 °C–r.t., 10 h; (c) Ar(CH<sub>2</sub>CH<sub>2</sub>)<sub>n</sub>NH<sub>2</sub>, Pd<sub>2</sub>(dba)<sub>3</sub>, Xtanphos, *t*-BuONa, 1,4-dioxane, 80 °C, 10 h; (d) 1-Methyl-4-[4-(4,4,5,5-tetramethyl-1,3,2-dioxaborolan-2-yl)benzyl]piperazine, Pd(PPh<sub>3</sub>)<sub>4</sub>, Na<sub>2</sub>CO<sub>3</sub>, 1,4-dioxane: H<sub>2</sub>O = 4: 1, 80 °C, 6 h; and (e) 4 M HCl in 1,4-dioxane, r.t., 4 h.



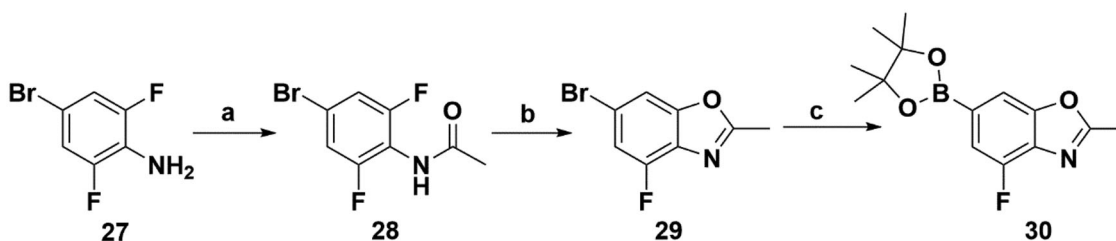
**Scheme 2.** Synthesis of target compounds **15a–15f**. Reagents and conditions: (a) Arylboric acid, Pd(PPh<sub>3</sub>)<sub>4</sub>, Na<sub>2</sub>CO<sub>3</sub>, 1,4-dioxane: H<sub>2</sub>O = 4: 1, 80 °C, 6 h; (b) 1-Methyl-4-[4-(4,4,5,5-tetramethyl-1,3,2-dioxaborolan-2-yl)benzyl]piperazine, Pd(PPh<sub>3</sub>)<sub>4</sub>, Na<sub>2</sub>CO<sub>3</sub>, 1,4-dioxane: H<sub>2</sub>O = 4: 1, 80 °C, 6 h; and (c) 4 M HCl in 1,4-dioxane, r.t., 4 h.



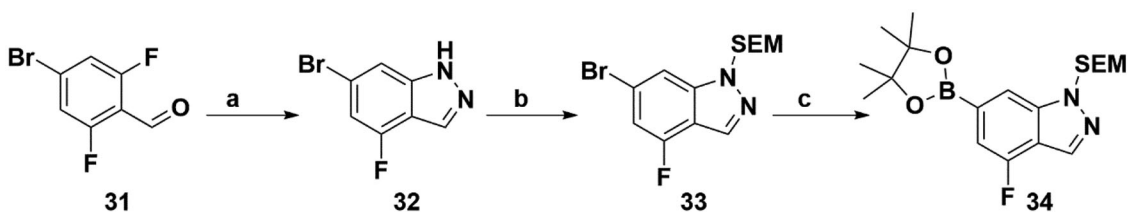
**Scheme 3.** Synthesis of target compounds 15g–15k. Reagents and conditions: (a) Fe, NH<sub>4</sub>Cl aq., 80 °C, 2 h; (b) HCOOH, reflux, 6 h; (c) Bis(pinacolato)diboron, Pd(dppf)Cl<sub>2</sub>, KOAc, 1,4-dioxane, 100 °C, 10 h; (d) Intermediate 9, Pd(PPh<sub>3</sub>)<sub>4</sub>, Na<sub>2</sub>CO<sub>3</sub>, 1,4-dioxane: H<sub>2</sub>O = 4: 1, 80 °C, 6 h; (e) Arylboric acid, Pd(PPh<sub>3</sub>)<sub>4</sub>, Na<sub>2</sub>CO<sub>3</sub>, 1,4-dioxane: H<sub>2</sub>O = 4: 1, 80 °C, 6 h; and (f) 4 M HCl in 1,4-dioxane, r.t., 4 h.



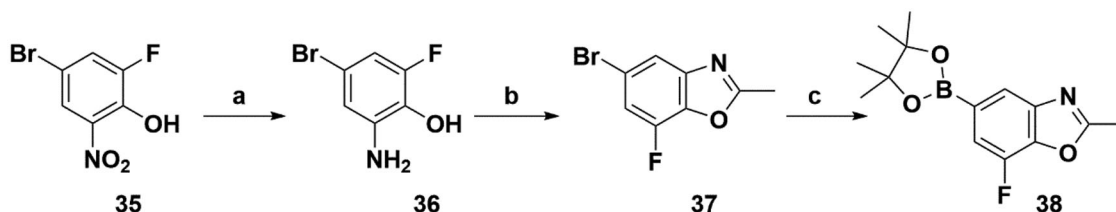
**Scheme 4.** Synthesis of the intermediate 26. Reagents and conditions: (a) i. TEA, Acetic anhydride, DCM, r.t., 8 h; ii. Et<sub>2</sub>O, K<sub>2</sub>CO<sub>3</sub>, r.t., 10 h; (b) 4-Bromo-2,6-difluoroaniline, POCl<sub>3</sub>, TEA, Toluene, reflux, 8 h; (c) *t*-BuOK, THF, 80 °C, 6 h; and (d) Bis(pinacolato)diboron, Pd(dppf)Cl<sub>2</sub>, KOAc, 1,4-dioxane, 100 °C, 10 h.



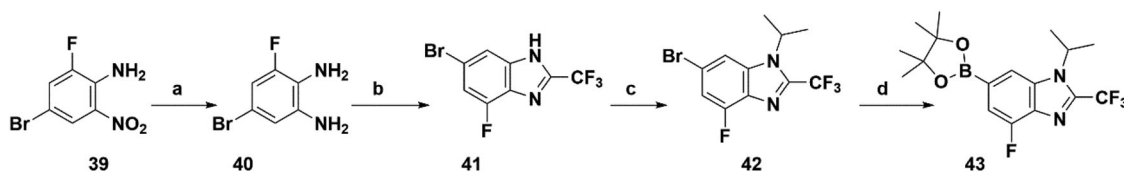
**Scheme 5.** Synthesis of the intermediate 30. Reagents and conditions: (a) Ac<sub>2</sub>O, AcOH, r.t., 5 h; (b) Cs<sub>2</sub>CO<sub>3</sub>, NMP, 150 °C, 10 h; and (c) Bis(pinacolato)diboron, Pd(dppf)Cl<sub>2</sub>, KOAc, 1,4-dioxane, 100 °C, 10 h.



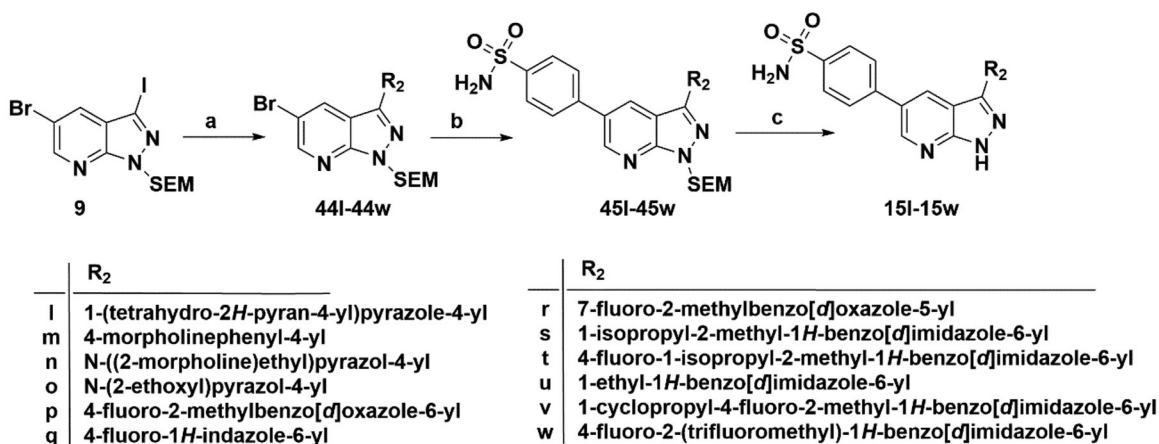
**Scheme 6.** Synthesis of the intermediate 34. Reagents and conditions: (a) N<sub>2</sub>H<sub>4</sub>·H<sub>2</sub>O, 1,4-dioxane, 90 °C, 5 h; (b) NaH, SEM-Cl, DMF, 0 °C–r.t., 10 h; and (c) Bis(pinacolato)diboron, Pd(dppf)Cl<sub>2</sub>, KOAc, 1,4-dioxane, 100 °C, 10 h.



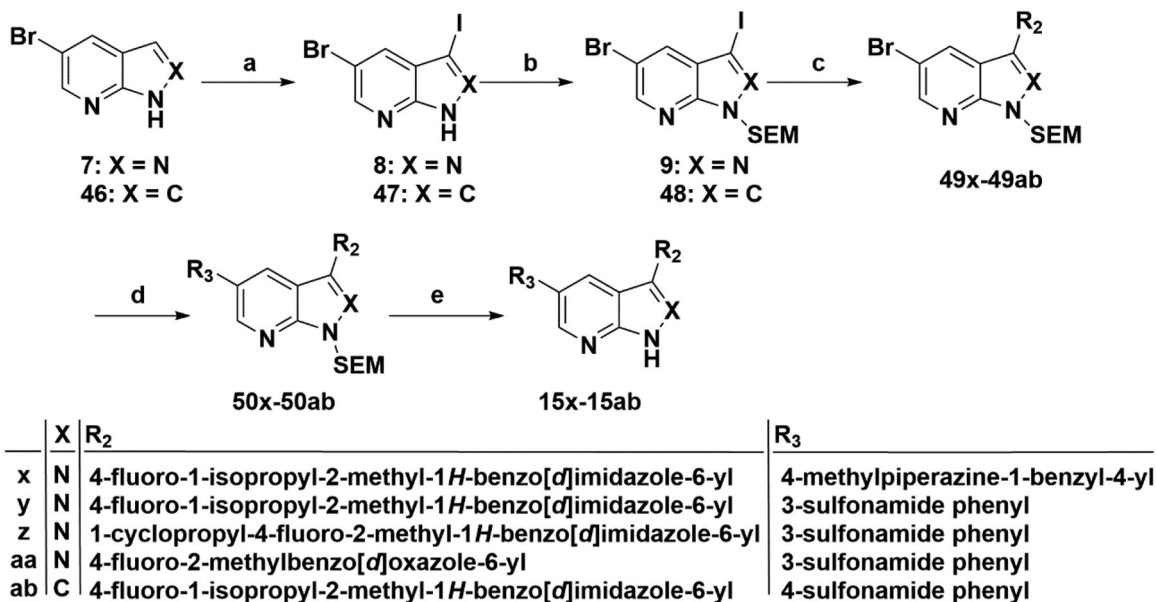
**Scheme 7.** Synthesis of the intermediate 38. Reagents and conditions: (a) Fe, NH<sub>4</sub>Cl aq., 80 °C, 2 h; (b) TMOA, 150 °C, 6 h; and (c) Bis(pinacolato)diboron, Pd(dppf)Cl<sub>2</sub>, KOAc, 1,4-dioxane, 100 °C, 10 h.



**Scheme 8.** Synthesis of the intermediate 43. Reagents and conditions: (a) Fe, NH<sub>4</sub>Cl aq., 80 °C, 2 h; (b) CF<sub>3</sub>COOH, 70 °C, 4 h; (c) NaH, SEM-Cl, DMF, 0 °C–r.t., 10 h; and (d) Bis(pinacolato)diboron, Pd(dppf)Cl<sub>2</sub>, KOAc, 1,4-dioxane, 100 °C, 10 h.



**Scheme 9.** Synthesis of target compounds 15l–15w. Reagents and conditions: (a) Arylboric acid, Pd(PPh<sub>3</sub>)<sub>4</sub>, Na<sub>2</sub>CO<sub>3</sub>, 1,4-dioxane: H<sub>2</sub>O = 4: 1, 80 °C, 6 h; (b) 4-(Aminosulfonyl) phenylboronic acid, Pd(PPh<sub>3</sub>)<sub>4</sub>, Na<sub>2</sub>CO<sub>3</sub>, 1,4-dioxane: H<sub>2</sub>O = 4: 1, 80 °C, 6 h; and (c) 4 M HCl in 1,4-dioxane, r.t., 4 h.



**Scheme 10.** Synthesis of target compounds 15x–15ab. Reagents and conditions: (a) NIS, DMF, 80 °C, 8 h; (b) NaH, SEM-Cl, DMF, 0 °C–r.t., 10 h; (c) Arylboric acid, Pd(PPh<sub>3</sub>)<sub>4</sub>, Na<sub>2</sub>CO<sub>3</sub>, 1,4-dioxane: H<sub>2</sub>O = 4: 1, 80 °C, 6 h; (d) Arylboric acid, Pd(PPh<sub>3</sub>)<sub>4</sub>, Na<sub>2</sub>CO<sub>3</sub>, 1,4-dioxane: H<sub>2</sub>O = 4: 1, 80 °C, 6 h; and (e) 4 M HCl in 1,4-dioxane, r.t., 4 h.

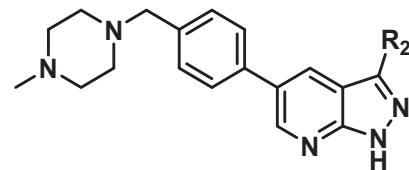
## 3.2. Biological evaluation

### 3.2.1. Target compounds design and in vitro activity against TBK1 kinase

The *in vitro* TBK1 inhibition activity of all the pyrazolo[3,4-b]pyridine derivatives was compared to the positive compounds **BX795** and **MRT67307**. The IC<sub>50</sub> value of all compounds could not be tested until the inhibition rate reached 50% at the concentration of 1 μM. Under our experimental conditions, **BX795** and

**MRT67307** exhibited TBK1 inhibition activity with IC<sub>50</sub> values of 7.1 nM and 28.7 nM, respectively, which was similar to previously reported data.

According to the binding mode of the above designed hit compound **6** (**15a**, 83.0% inhibition @ 10 μM) and TBK1, we first synthesised first-series nine pyrazolo[3,4-b]pyridine compounds **12a–12i** by fragment splicing strategy to introduce the alkylamino side chain of **BX795**, which were characterised by replacing indole ring with 1–3 carbon-length alkylamino fragments at R<sub>2</sub> position.

**Table 1.** *In vitro* TBK1 kinase inhibitory activity of the **12a–12i**, **15a–15f**.<sup>a</sup>


Compound	R <sub>2</sub>	TBK1 inhibition (%)				IC <sub>50</sub> /nM
		10 μM	1 μM	100 nM	10 nM	
<b>12a</b>		-8.0	-13.6	-14.5	N.T. <sup>b</sup>	N.T.
<b>12b</b>		3.2	5.9	7.3	N.T.	N.T.
<b>12c</b>		-2.0	-6.7	-30.1	N.T.	N.T.
<b>12d</b>		-4.7	-5.8	-5.6	N.T.	N.T.
<b>12e</b>		-5.0	-2.4	-1.4	N.T.	N.T.
<b>12f</b>		-0.5	-7.9	-9.7	N.T.	N.T.
<b>12g</b>		-4.9	-5.2	-6.2	N.T.	N.T.
<b>12h</b>		-5.2	-4.3	-7.8	N.T.	N.T.
<b>12i</b>		7.1	19.9	15.2	16.2	N.T.
<b>15a</b>		83.0	36.5	13.2	N.T.	N.T.
<b>15b</b>		47.9	14.3	11.0	N.T.	N.T.
<b>15c</b>		86.8	47.8	38.3	N.T.	N.T.
<b>15d</b>		102.2	84.1	52.5	18.0	130.6
<b>15e</b>		107.6	103.9	62.8	14.3	75.3
<b>15f</b>		101.4	81.4	28.7	N.T.	290.4
<b>BX795</b>		N.T.	N.T.	99.6	72.9	7.1
<b>MRT67307</b>		N.T.	N.T.	92.8	29.6	28.7

<sup>a</sup>The IC<sub>50</sub> values are shown as the mean (nM) values from two separate experiments.

<sup>b</sup>N.T. = not tested.

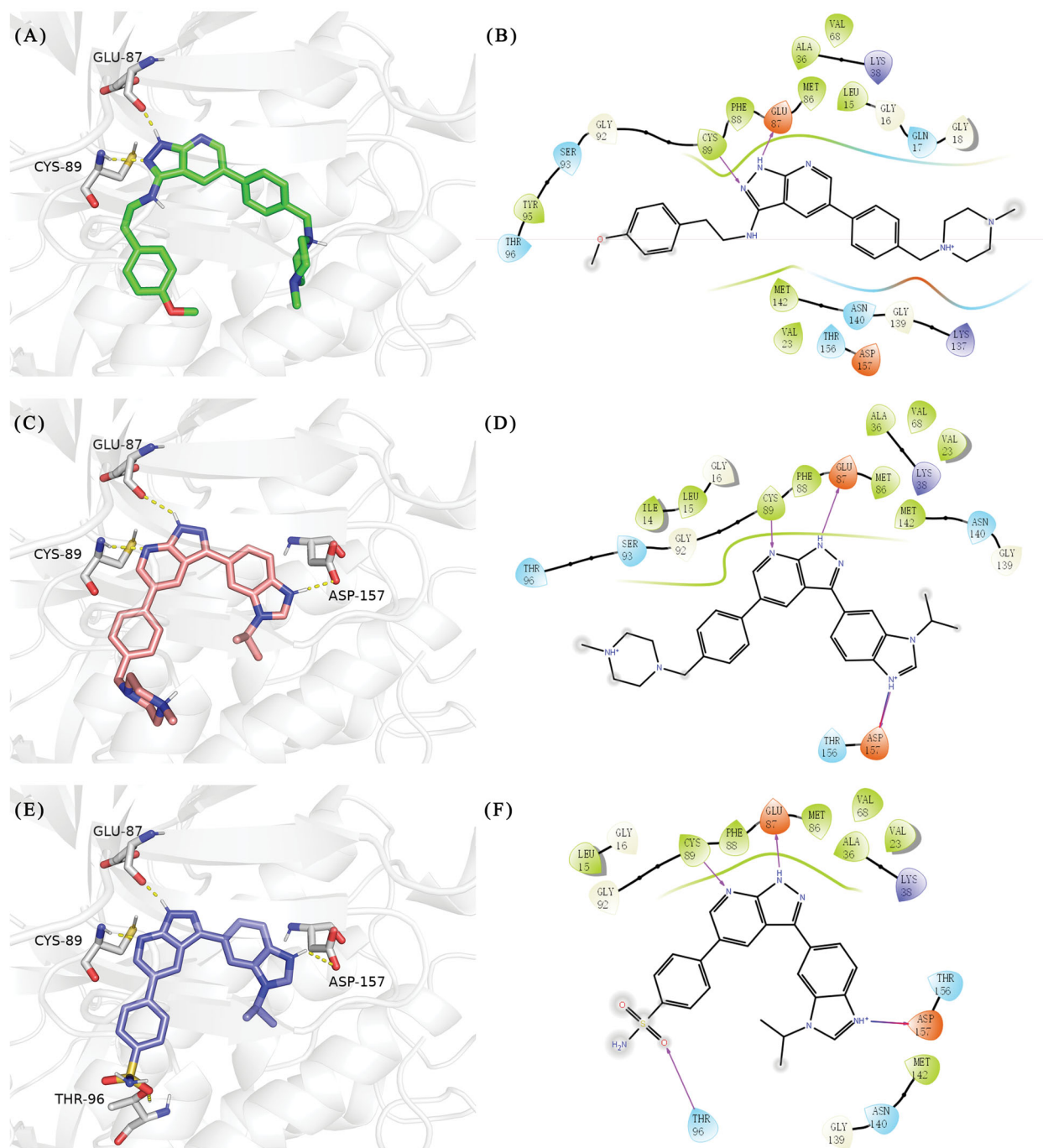
Unfortunately, as shown in **Table 1**, all the compounds designed above exhibited no significant inhibitory activity on TBK1 regardless of the electron-withdrawing or electron-donating substituents on the aromatic ring. We speculated the reason for the loss of

their activities as follows: take compound **12f** as an example, the docking study indicated that N and NH of pyrazole moiety in **12f** replacing pyridine N and pyrazole NH of pyrazolopyridine moiety formed two hydrogen bonds with Glu87 and Cys89 in hinge region of the TBK1, which completely reversed the binding model between molecule and protein, thus making methylpiperazine extend to DFG region away from solvent region (**Figure 4(A,B)**).

In addition, in order to explore the importance of hydrogen bond between Asp157 and indole of compound **6**, we also synthesised and tested the inhibitory activity of the second-series five pyrazolo[3,4-b]pyridine compounds **15b–15f**, and the result was shown in **Table 1**. Considering that Asp157 was an acidic amino acid, we expected to increase the basicity of N atom and form a salt bridge with Asp157 to further enhance the receptor-ligand interaction. The indole ring of compound **15a** was opened to obtain aniline (**15c**) which slightly improved the activity. However, the activity of compound **15b** decreased significantly, which might be explained by meta-aniline far away from Asp157. When indole was substituted by benzimidazole or isoquinoline with stronger basicity, the activities of **15d** and **15f** were obviously increased. And a potent lead compound **15e** (IC<sub>50</sub> = 75.3 nM) was confirmed by introducing isopropyl to the N atom of benzimidazole. The docking study showed that imidazole of **15e** and Asp157 formed a salt bridge (**Figure 4(C,D)**). We concluded that Asp157 was an important amino acid for TBK1-dependent activity and it was also significant to introduce hydrophobic fragments into the hydrophobic cavity adjacent to the DFG motif.

After further studying the distribution of amino acids in the active cavity, we found that there were some amino acids such as Thr96, Ser93, and Leu15 in the solvent region that could form hydrogen bonds with ligands. Therefore, different hydrophilic fragments were introduced in R<sub>3</sub> moiety of **15e** to obtain compounds **15g–15k** (**Table 2**). Except compound **15k** (IC<sub>50</sub> = 287.7 nM), the IC<sub>50</sub> value of other compounds was less than 100 nM, among which compound **15i** (IC<sub>50</sub> = 8.5 nM) displayed potent inhibition activity and the IC<sub>50</sub> value was nearly 10 times lower than compound **15e**. The docking study of compound **15i** was showed (**Figure 4(E,F)**), and the oxygen atom of sulphonamide could form hydrogen bond with Ser96, which might be the main reason of the further improvement of activity.

For further exploring the SARs, we fixed the benzene sulphonamide fragment of R<sub>3</sub> and investigated the influence of R<sub>2</sub> on the activity according to the following three points: (1) Substitution of benzopyrazole ring by monocyclic or other bicyclic rings; (2) introducing substituents into benzimidazole ring; and (3) replacing isopropyl with other alkyl fragments. The *in vitro* kinase assays with compounds **15l–15w** were illustrated in **Table 3**. Compounds **15l–15r** including different substituted rings that did not form hydrogen bond with Asp157 decreased obviously, which further confirmed that Asp157 was an important amino acid in maintaining TBK1 activity. Compound **15s** replaced hydrogen atom with methyl at imidazole 2 position, and its activity remained unchanged. The activity of compound **15t** was further enhanced (IC<sub>50</sub> = 0.8 nM) by introducing fluorine atom into benzene ring and was increased by 10 times compared with compound **15i**. The potency improvement of compound **15t** might be explained by the fluorine atom could form a hydrogen bond with Lys38 (**Figure 5(A,B)**). Compared to compounds **15i** and **15t**, introduction of ethyl and cyclopropyl (**15u** and **15v**) at the nitrogen atom of pyrazole moiety resulted in a slight decline in activity, indicating that isopropyl was the more suitable to occupy the hydrophobic cavity beside DFG motif. Compound **15w** with trifluoromethyl replacing methyl almost lost TBK1 activity. Based on the above

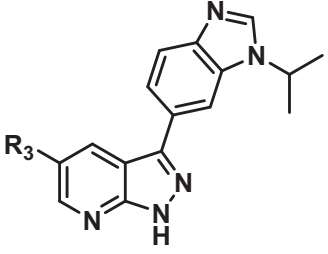


**Figure 4.** (A) The binding mode of **12f** (coloured by element with carbons in green) in the TBK1 active site. (B) 2D diagram of the interaction between compound **12f** and TBK1. (C) The binding mode of **15e** (coloured by element with carbons in salmon pink) in the TBK1 active site. (D) 2D diagram of the interaction between compound **15e** and TBK1. (E) The binding mode of **15i** (coloured by element with carbons in slate) in the TBK1 active site. (F) 2D diagram of the interaction between compound **15i** and TBK1. The kinase was depicted in white cartoon, and interactions were illustrated with yellow dashed lines.

results, we have gained a potent TBK1 inhibitor **15t** superior to positive compounds.

In the last round of structural modification, guided by molecular docking, we discovered that the ligand could form hydrogen bonds with Thr96 and Leu15 simultaneously in solvent region after para-sulphonamide was transferred to meta-position. Compared with compound **15t**, the activity of compound **15y** ( $IC_{50} = 0.2 \text{ nM}$ ) further increased by four times (Table 4), and the docking result was shown in Figure 5(C,D). Protonated N of benzimidazole ring formed a salt bridge with Asp157 of DFG motif, and fluorine atom formed a hydrogen bond with Lys38; Two hydrogen bonds were formed between NH and N of pyrazolopyridine and

hinge region residues Glu87 and Cys89, respectively; NH and O of benzene sulphonamide formed two hydrogen bonds with solvent region residues Leu15 and Thr96, respectively, helping to explain the high affinity imparted by this moiety. Furthermore, we also verified that benzene sulphonamide fragment (**15y**) in solvent region was superior to methylpiperazine (**15x**), isopropyl on nitrogen atom was superior to cyclopropyl (**15z**), and trifluoromethyl substitution (**15aa**) was unfavourable for activity. Consistent with the previous analysis, when the N atom was replaced by C atom, compound **15ab** showed 8-fold reduced activity against TBK1 compared to **15t**. Finally, the most potent TBK1 inhibitor **15y** was selected for further biological evaluation.

**Table 2.** *In vitro* TBK1 kinase inhibitory activity of the 15g–15k.<sup>a</sup>


Compound	R <sub>3</sub>	TBK1 inhibition (%)					IC <sub>50</sub> /nM
		10 μM	1 μM	100 nM	10 nM	1 nM	
15g		107.8	108.5	91.7	29.9	8.6	26.0
15h		103.4	103.5	75.6	29.1	24.0	58.9
15i		110.7	104.6	75.4	62.3	47.3	8.5
15j		102.9	104.5	67.1	31.5	14.2	67.2
15k		106.3	82.6	45.0	19.5	N.T. <sup>b</sup>	287.7
BX795		N.T.	N.T.	99.6	72.9	37.7	7.1
MRT67307		N.T.	N.T.	92.8	29.6	2.4	28.7

<sup>a</sup>The IC<sub>50</sub> values are shown as the mean (nM) values from two separate experiments.

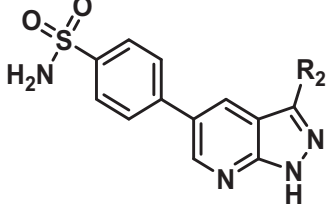
<sup>b</sup>N.T. = not tested.

### 3.2.2. Structure–activity relationships

The SARs study of the novel compounds was represented in Figure 6. Starting from hit compound **6**, two-series compounds were obtained based on rational design. In the first series, when indole ring was replaced by aryl aliphatic amines with 1–3 carbon length, no matter whether the aromatic ring was an electron-withdrawing or electron-donating substituent, these compounds did not show obvious TBK1 inhibitory activity. In the second series, benzene sulphonamide substitution on pyridine ring contributed greatly to the activity, and meta-sulphonamide was better than para-sulphonamide. The benzimidazole substitution in the R part of pyrazole ring was superior to other bicyclic and monocyclic substitutions. And when R<sup>3</sup> = isopropyl, R<sup>4</sup> = methyl, TBK1 could be strongly inhibited. When R<sup>5</sup> was a fluorine atom, the inhibitory activity of compounds on TBK1 could be significantly enhanced. When the nucleus skeleton was 1*H*-pyrazolo[3,4-*b*]pyridine or 1*H*-pyrrolo[2,3-*b*]pyridine, the inhibitory activity against TBK1 was equivalent, which proved that pyridine N and pyrazole NH, rather than pyrazole N and NH, played an anchoring role in the hinge region.

### 3.2.3. Kinase selectivity profile

The potent compound **15y** was subjected to kinase selectivity profiling against a panel of 31 kinases at a concentration of 1.0 μM to further evaluate the selectivity of this series, and the enzyme activity results were given in Figure 7 and Table 5. We

**Table 3.** *In vitro* TBK1 kinase inhibitory activity of the 15l–15w.<sup>a</sup>


Compound	R <sub>2</sub>	TBK1 inhibition (%)							IC <sub>50</sub> /nM
		10 μM	1 μM	100 nM	10 nM	1 nM	0.1 nM		
15l		21.9	−0.6	−7.2	N.T. <sup>b</sup>	N.T.	N.T.	N.T.	N.T.
15m		−11.0	−6.0	−8.9	N.T.	N.T.	N.T.	N.T.	N.T.
15n		−12.5	−15.0	−8.9	N.T.	N.T.	N.T.	N.T.	N.T.
15o		23.3	−7.4	−2.7	N.T.	N.T.	N.T.	N.T.	N.T.
15p		41.1	37.1	30.6	32.0	N.T.	N.T.	N.T.	N.T.
15q		83.9	25.5	12.7	4.5	N.T.	N.T.	N.T.	N.T.
15r		56.8	5.7	10.8	−2.6	N.T.	N.T.	N.T.	N.T.
15s		N.T.	97.2	76.9	68.6	45.5	N.T.	6.2	
15t		N.T.	99.1	79.5	78.0	61.6	43.1	0.8	
15u		N.T.	89.6	78.1	30.0	25.1	12.1	33.3	
15v		N.T.	87.4	70.3	49.7	42.5	37.7	31.2	
15w		N.T.	N.T.	27.1	10.7	N.T.	N.T.	N.T.	
BX795		N.T.	N.T.	99.6	72.9	37.7	0.18	7.1	
MRT67307		N.T.	N.T.	92.8	29.6	2.4	<0	28.7	

<sup>a</sup>The IC<sub>50</sub> values are shown as the mean (nM) values from two separate experiments.

<sup>b</sup>N.T. = not tested.

could see that TBK1, IKKε, IKKα, MLK1, and Aurora A were produced less than 20% kinase activity (red columns in Figure 6) by compound **15y**, the activity of eight kinases (CK1γ1, PKCθ, IKKβ, PI3K(p120g), mTOR, ALK, PKCα, and PDGFRβ) ranged from 20% to

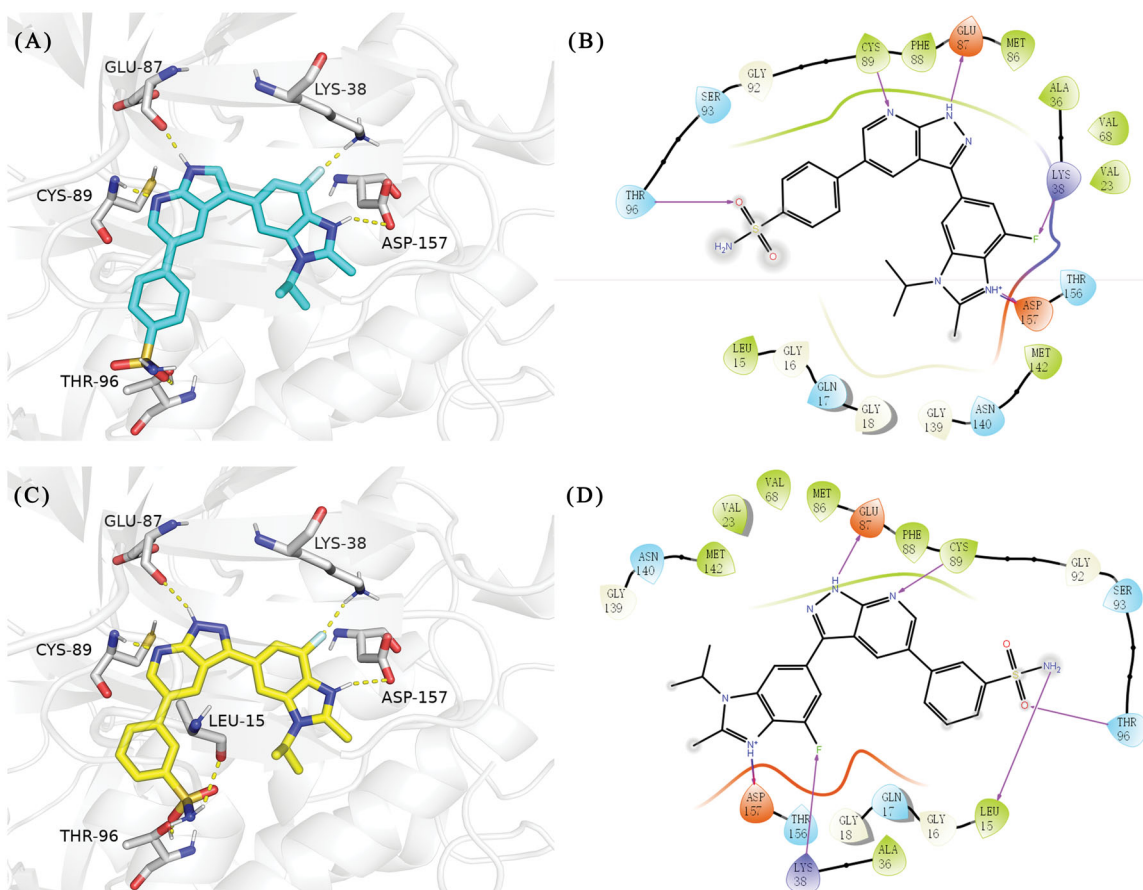


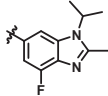
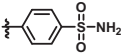
**Figure 5.** (A) The binding mode of **15t** (coloured by element with carbons in cyan) in the TBK1 active site. (B) 2D diagram of the interaction between compound **15t** and TBK1. (C) The binding mode of **15y** (coloured by element with carbons in yellow) in the TBK1 active site. (D) 2D diagram of the interaction between compound **15y** and TBK1. The kinase was depicted in white cartoon, and interactions were illustrated with yellow dashed lines.

**Table 4.** *In vitro* TBK1 kinase inhibitory activity of the **15x–15ab**.<sup>a</sup>

Compd.	X	R <sub>2</sub>	R <sub>3</sub>	TBK1 inhibition (%)					IC <sub>50</sub> /nM
				1 μM	100 nM	10 nM	1 nM	0.1 nM	
<b>15x</b>	N			75.8	80.5	34.1	18.6	N.T.	22.0
<b>15y</b>	N			53.9	102.4	93.8	88.8	33.6	0.2
<b>15z</b>	N			79.5	84.4	48.4	32.7	N.T.	24.4
<b>15aa</b>	N			48.3	36.8	14.10	N.T. <sup>b</sup>	N.T.	N.T.

(continued)

Table 4. Continued.

Compd.	X	R <sub>2</sub>	R <sub>3</sub>	TBK1 inhibition (%)					IC <sub>50</sub> /nM
				1 μM	100 nM	10 nM	1 nM	0.1 nM	
15ab	C			90.3	72.9	70.9	60.1	43.1	3.6
BX795				N.T.	99.6	72.9	37.7	0.18	7.1
MRT67307				N.T.	92.8	29.6	2.4	<0	28.7

<sup>a</sup>The IC<sub>50</sub> values are shown as the mean (nM) values from two separate experiments.

<sup>b</sup>N.T. = not tested.

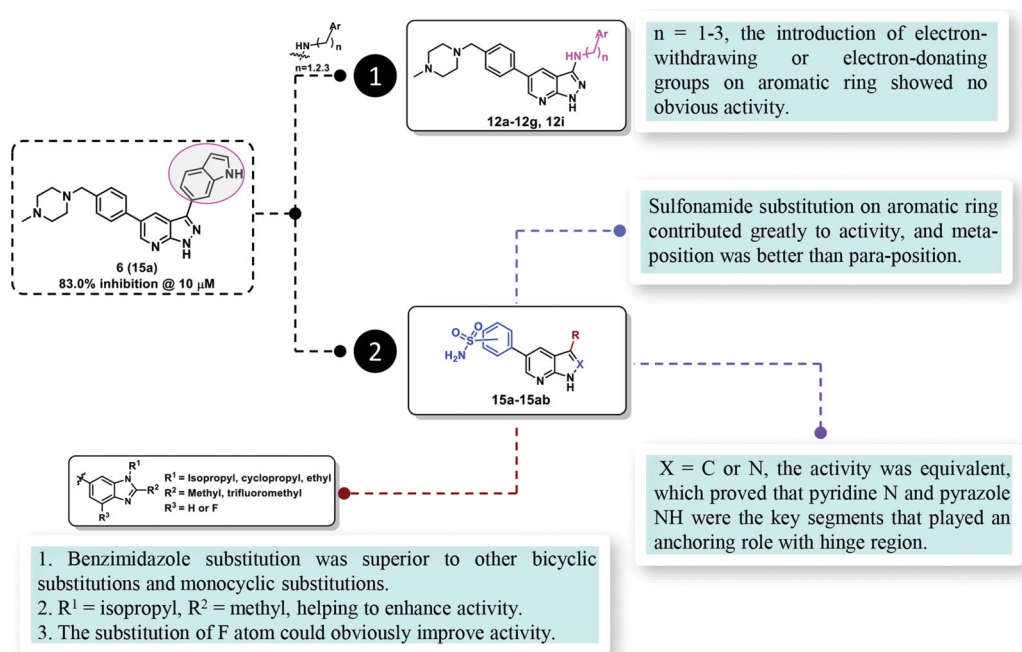


Figure 6. The structure–activity relationships of the designed novel compounds.

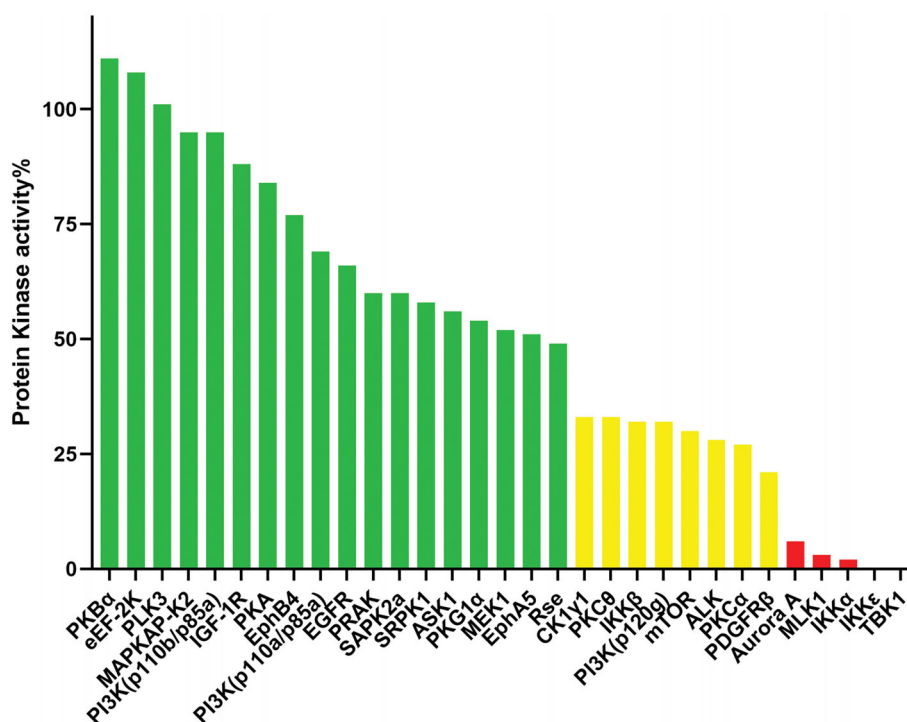


Figure 7. Selectivity profile of compound 15y measured at a concentration of 1.0 μM in a panel of 31 kinases (red columns denote <20%, yellow columns denote between 20% and 40% and green columns denote >40%).

**Table 5.** Kinase selectivity profile of compound **15y**.<sup>a</sup>

Kinases	%kinase activity @ 1.0 μM	Kinases	%kinase activity @ 1.0 μM	Kinases	%kinase activity @ 1.0 μM
PKBα	111	SAPK2a	60	mTOR	30
eEF-2K	108	SRPK1	58	ALK	28
PLK3	101	ASK1	56	PKCα	27
MAPKAP-K2	95	PKG1α	54	PDGFRβ	21
PI3K(p110b/p85a)	95	MEK1	52	Aurora A	6
IGF-1R	88	EphA5	51	MLK1	3
PKA	84	Rse	49	IKKα	2
EphB4	77	CK1γ1	33	IKKε	-1
PI3K(p110a/p85a)	69	PKCθ	33	TBK1	-2
EGFR	66	IKKβ	32		
PRAK	60	PI3K(p120g)	32		

Profiling Service from Life Technologies. The results represent the mean of three independent experiments performed in triplicate.

<sup>a</sup>Selectivity profile of compound **15y** was measured at a concentration of 1.0 μM in a panel of 31 kinases generated with the SelectScreen®.

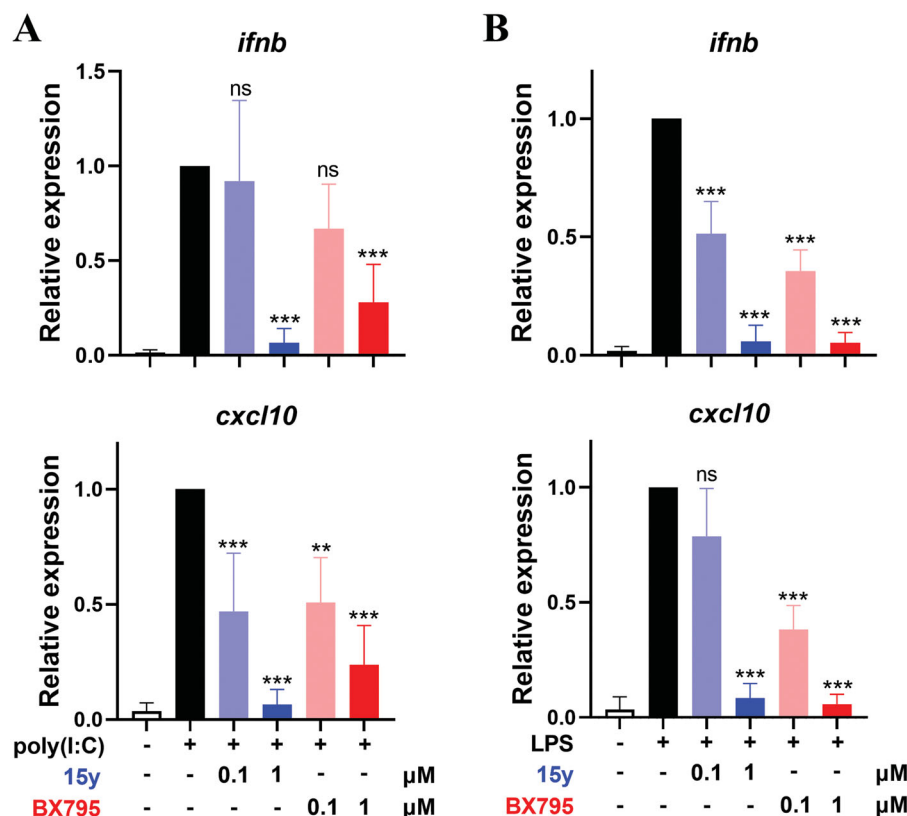


**Figure 8.** Compound **15y** inhibited the expression of *ifnb* and *cxcl10* genes expression in THP-1 cells (A) and RAW264.7 cells (B), stimulated by poly(I:C) or LPS, respectively. Data are representative of at least 3 independent experiments and are shown in mean  $\pm$  SD value. The significance of the differences between poly(I:C) or LPS stimulation-only group and the stimulation plus compound treated groups were determined by One-Way ANOVA test. \*\* $p < .01$ ; \*\*\* $p < .001$ ; ns, not significant.

40% (yellow columns in Figure 7), and the other 18 kinases activity was greater than 40% (green columns in Figure 7).

### 3.2.4. mRNA detection of TBK1 downstream genes

Based on the potent kinase inhibitory activity and the acceptable selectivity of compound **15y**, we subsequently analysed its cellular TBK1 inhibitory activity. As it is well recognised that innate immune stimuli poly(I:C) and LPS are enable of activating TBK1-IRF3 pathway and therefore triggering a boosted expression of several IFN gene expression, such as *ifnb* and *cxcl10*<sup>3</sup>, we examined the activities of compound **15y** on the expression of *ifnb* and *cxcl10* stimulated by poly(I:C) or LPS in THP-1 and RAW264.7 monocytes. As shown in Figure 8, *ifnb* and *cxcl10* gene expression were both activated in these cells. As expected, compound **15y** treatment inhibited this robustly increased *ifnb* and *cxcl10*

expression in THP-1 cells in a dose-dependent manner (Figure 8(A)), and achieved an almost complete inhibition at the concentration of 1 μM (both >93% inhibition), while **BX795** exhibited a much weaker effect at the same concentration. Similar results were also observed in LPS-stimulated murine RAW264.7 cells with a profound activity of compound **15y** (Figure 8(B)). These results confirmed that compound **15y** effectively inhibited TBK1 downstream IFN signalling in cells.

### 3.2.5. Antiproliferative activity of compound 15y

TBK1 is central to multiple biological processes in cancer progression, and pharmacological targeting TBK1 has been reported to induced a context-selective impairment of tumourigenesis in glioma,<sup>15</sup> melanoma,<sup>16</sup> pancreatic cancer,<sup>17-18</sup> and other cancers. We therefore explored the anti-tumour proliferation effect of

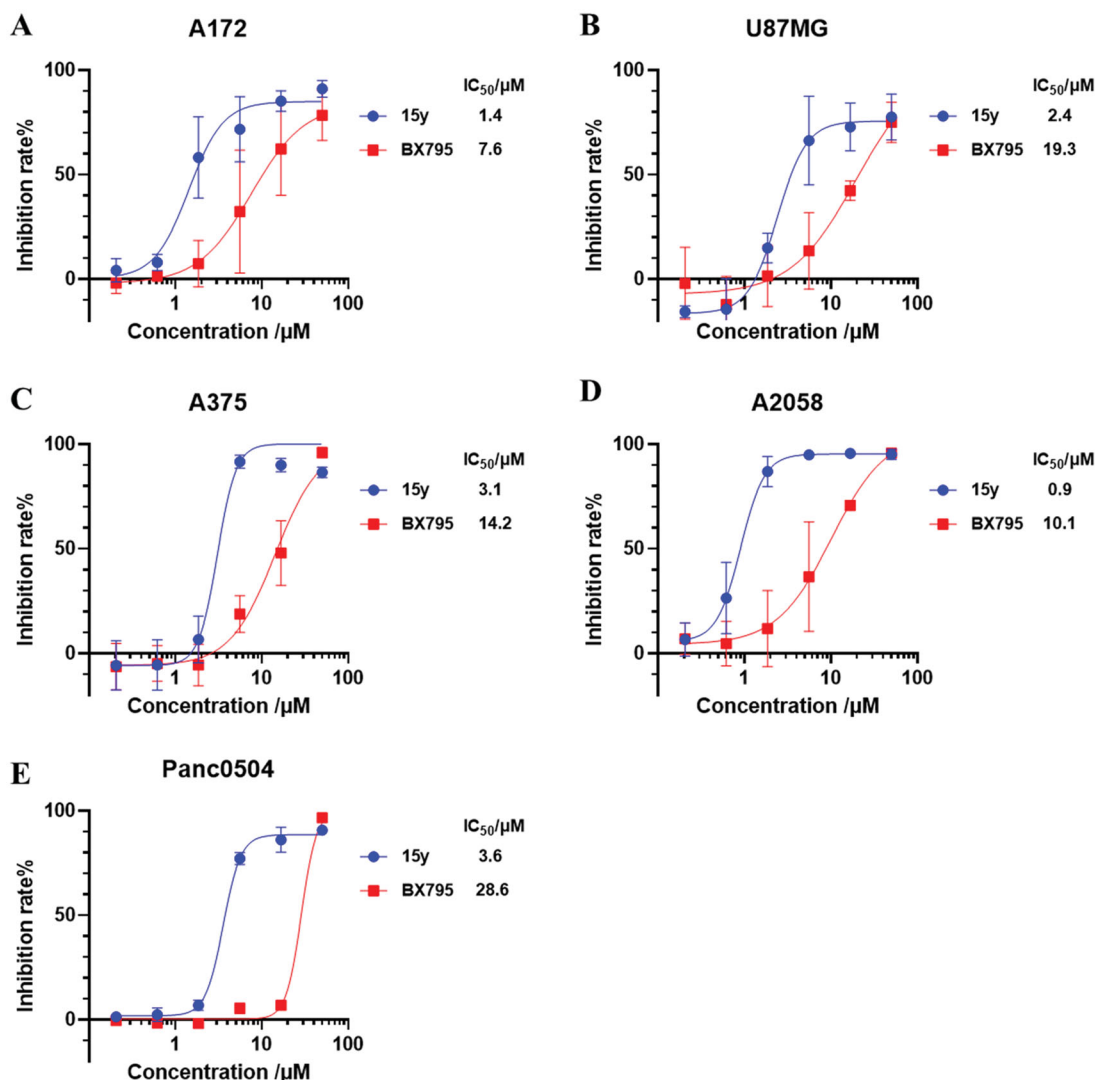


**Figure 9.** Compound **15y** inhibited the viability of two glioma cell lines A172 and U87MG (A, B), two melanoma cell lines A375 and A2058 (C, D), and one pancreatic cell line Panc0504 (E). Cell viability were measured by SRB staining method 72 h after cells treated by increasing doses of compound **15y** and **BX795**. Data are representative of three independent experiments and are shown in mean  $\pm$  SD value. Nolin fit four-parameters model were used to fit the curve and to calculate IC<sub>50</sub> values by GraphPad 8.0.

compound **15y** in different types of cancer cells, including two glioma cell lines (A172 and U87MG), two melanoma cell lines (A375 and A2058), and one pancreatic cell line (Panc0504). As demonstrated in Figure 9(A,B), compound **15y** exhibited a profound antiproliferative effect in both glioma cell lines with average IC<sub>50</sub> values of 1.4  $\mu$ M in A172 cells and 2.4  $\mu$ M in U87MG cells. It also effectively inhibited the proliferation of A375, A2058 and Panc0504 cell lines, with IC<sub>50</sub> values of 3.1  $\mu$ M, 0.9  $\mu$ M, and 3.6  $\mu$ M, respectively (Figure 9(C-E)). In contrast, **BX795** only modestly impaired the viability of these cancer cells with IC<sub>50</sub> values ranging between 7.6  $\mu$ M and 28.6  $\mu$ M, showing much weaker effects than compound **15y** (Figure 9(A-E)). It is worth mentioned that the antiproliferative activity of compound **15y** may not fully resulted from TBK1 inhibition due to its modest selectivity (see Figure 7 and Table 5); however, these results did suggest compound **15y** could serve as a potent anti-tumour agent. Moreover, human umbilical vein endothelial cells (HUVECs) were used to evaluate the cytotoxicity of compound **15y** to normal cells (Figure S1). The result indicated that compound **15y** showed weak toxicity to HUVECs with an IC<sub>50</sub> value of 21.2  $\mu$ M.

#### 4. Conclusion

By analysing the binding modes of compound **URMC-099** and TBK1, we utilised the bioisostere strategy to obtained a series of 1*H*-pyrazolo[3,4-*b*]pyridine derivatives based on computer-aided drug design (CADD). The *in vitro* enzyme activity assays suggested the optimised compound **15y** exhibited picomolar inhibitory activity against TBK1 with an IC<sub>50</sub> value of 0.2 nM. And the kinase selectivity profiling of compound **15y** presented good kinase selectivity. Subsequently, we proved that compound **15y** sufficiently inhibited the mRNA expression of TBK1-downstream genes in stimulated THP-1 and RAW264.7 cells. Also, compound **15y** exhibited a profound antiproliferation effect on A172, U87MG, A375, A2058, and Panc0504 cell lines with the IC<sub>50</sub> of micromole level, which was significantly effective than **BX795**. These results indicate that compound **15y** is a novel, highly potent TBK1 inhibitor with predominant bioactivity and is predicted to be a promising tool compound that is helpful to understand functions of targeting TBK1 in immune response and cancer therapy.

## Acknowledgements

We gratefully acknowledge the Program for Innovative Research Team of the Ministry of Education and the Program for Liaoning Innovative Research Team in University.

## Disclosure statement

The authors declare no competing financial interest.

## Funding

We are grateful for financial support from the Lingang Laboratory Grant (LG202103-02-01 and LG202103-02-02) and the National Natural Science Foundation of China [Grant 82173658 and 81773572].

## References

- Revach OY, Liu S, Jenkins RW. Targeting tank-binding kinase 1 (tbk1) in cancer. *Expert Opin Ther Targets* 2020;24:1411–78.
- Zhou R, Zhang Q, Xu P. Tbk1, a central kinase in innate immune sensing of nucleic acids and beyond. *Acta Biochim Biophys Sin* 2020;52:757–67.
- Xiang S, Song S, Tang H, et al. Tank-binding kinase 1 (TBK1): an emerging therapeutic target for drug discovery. *Drug Discov Today* 2021;26:2445–55.
- Lee DF, Hung MC. Advances in targeting IKK and IKK-related kinases for cancer therapy. *Clin Cancer Res* 2008;14:5656–62.
- Larabi A, Devos JM, Ng SL, et al. Crystal structure and mechanism of activation of tank-binding kinase 1. *Cell Rep* 2013;3:734–46.
- Muvaffak A, Pan Q, Yan H, et al. Evaluating TBK1 as a therapeutic target in cancers with activated IRF3. *Mol Cancer Res* 2014;12:1055–66.
- Louis C, Burns C, Wicks I. Tank-binding kinase 1-dependent responses in health and autoimmunity. *Front Immunol* 2018;9:434.
- Marion JD, Roberts CF, Call RJ, et al. Mechanism of endogenous regulation of the type I interferon response by suppressor of  $\kappa$ B kinase epsilon (SIKE), a novel substrate of TANK-binding kinase 1 (TBK1). *J Biol Chem* 2013;288:18612–23.
- Yu T, Yang Y, Yin DQ, et al. TBK1 inhibitors: a review of patent literature (2011–2014). *Expert Opin Ther Pat* 2015;25:1385–96.
- Chen Q, Sun L, Chen ZJ. Regulation and function of the cGAS-STING pathway of cytosolic DNA sensing. *Nat Immunol* 2016;17:1142–9.
- Wang X, Teng F, Lu J, et al. Expression and prognostic role of IKBKE and TBK1 in stage I non-small cell lung cancer. *Cancer Manag Res* 2019;11:6593–602.
- Wei C, Cao Y, Yang X, et al. Elevated expression of tank-binding kinase 1 enhances tamoxifen resistance in breast cancer. *Proc Natl Acad Sci USA* 2014;111:E601–610.
- Shen RR, Hahn WC. Emerging roles for the non-canonical IKKs in cancer. *Oncogene* 2011;30:631–41.
- Chen W, Luo K, Ke Z, et al. TBK1 promote bladder cancer cell proliferation and migration via Akt signaling. *J Cancer* 2017;8:1892–9.
- Scuderi SA, Lanza M, Casili G, et al. TBK1 inhibitor exerts antiproliferative effect on glioblastoma multiforme cells. *Oncol Res* 2021;28:779–90.
- Eskioçak B, McMillan EA, Mendiratta S, et al. Biomarker accessible and chemically addressable mechanistic subtypes of BRAF melanoma. *Cancer Discov* 2017;7:832–51.
- Yasui L, Baker N, Savage H, Der C. Ultrastructure of human pancreatic cancer cells treated with a TBK1 inhibitor. *Microsc Microanal* 2019;25:1284–5.
- Yang S, Imamura Y, Jenkins RW, et al. Autophagy inhibition dysregulates TBK1 signaling and promotes pancreatic inflammation. *Cancer Immunol Res* 2016;4:520–30.
- Barbie DA, Tamayo P, Boehm JS, et al. Systematic RNA interference reveals that oncogenic KRAS-driven cancers require TBK1. *Nature* 2009;462:108–12.
- Clark K, Plater L, Peggie M, Cohen P. Use of the pharmacological inhibitor BX795 to study the regulation and physiological roles of TBK1 and I $\kappa$ B kinase epsilon: a distinct upstream kinase mediates ser-172 phosphorylation and activation. *J Biol Chem* 2009;284:14136–46.
- Yu T, Wang Z, Jie W, et al. The kinase inhibitor bx795 suppresses the inflammatory response via multiple kinases. *Biochem Pharmacol* 2020;174:113797.
- Tu D, Zhu Z, Zhou AY, et al. Structure and ubiquitination-dependent activation of tank-binding kinase 1. *Cell Rep* 2013;3:747–58.
- Clark K, Peggie M, Plater L, et al. Novel cross-talk within the IKK family controls innate immunity. *Biochem J* 2011;434:93–104.
- Petherick KJ, Conway OJ, Mpamhanga C, et al. Pharmacological inhibition of ULK1 kinase blocks mammalian target of rapamycin (mTOR)-dependent autophagy. *J Biol Chem* 2015;290:11376–83.
- Jenkins RW, Aref AR, Lizotte PH, et al. Ex vivo profiling of PD-1 blockade using organotypic tumor spheroids. *Cancer Discov* 2018;8:196–215.
- Thomson DW, PoECKel D, Zinn N, et al. Discovery of GSK8612, a highly selective and potent TBK1 inhibitor. *ACS Med Chem Lett* 2019;10:780–5.
- Lefranc J, Schulze VK, Hillig RC, et al. Discovery of BAY-985, a highly selective TBK1/IKK $\epsilon$  inhibitor. *J Med Chem* 2020;63:601–12.
- Nam Y, Hwang D, Kim N, et al. Identification of 1H-pyrazolo [3,4-b]pyridine derivatives as potent ALK-L1196M inhibitors. *J Enzyme Inhib Med Chem* 2019;34:1426–38.
- Pfaffenrot B, Klovekorn P, Juchum M, et al. Design and synthesis of 1H-pyrazolo[3,4-b]pyridines targeting mitogen-activated protein kinase 4 (MKK4) - a promising target for liver regeneration. *Eur J Med Chem* 2021;218:113371.